



OPEN ACCESS

EDITED BY

Natalia V. Kirienko,
Rice University, United States

REVIEWED BY

Rossella Labella,
Columbia University, United States
Jie Wang,
First Affiliated Hospital of Xinjiang Medical
University, China

*CORRESPONDENCE

Xiaoli Wu

✉ sjzwxl19730608@163.com

RECEIVED 20 February 2025

ACCEPTED 24 July 2025

PUBLISHED 12 August 2025

CITATION

Xuan F, Zhu WY, Zhang BX, Zhao H, Li CN
and Wu XL (2025) Identification of the
prognostic effect of mitophagy-related
genes in acute myeloid leukemia.
Front. Immunol. 16:1580597.
doi: 10.3389/fimmu.2025.1580597

COPYRIGHT

© 2025 Xuan, Zhu, Zhang, Zhao, Li and Wu.
This is an open-access article distributed under
the terms of the [Creative Commons Attribution
License \(CC BY\)](#). The use, distribution or
reproduction in other forums is permitted,
provided the original author(s) and the
copyright owner(s) are credited and that the
original publication in this journal is cited, in
accordance with accepted academic
practice. No use, distribution or reproduction
is permitted which does not comply with
these terms.

Identification of the prognostic effect of mitophagy-related genes in acute myeloid leukemia

Fan Xuan¹, Wenyuan Zhu², Baoxi Zhang¹, Hui Zhao¹,
Chaonan Li¹ and Xiaoli Wu^{1*}

¹Department of Pediatrics, Hematology and Oncology, Second Hospital of Hebei Medical University, Shijiazhuang, China, ²Graduate School, Hebei Medical University, Shijiazhuang, Hebei, China

Background: Mitophagy has been implicated in the pathogenesis of acute myeloid leukemia (AML), yet its precise molecular mechanisms remain poorly understood. Understanding the roles of mitophagy-related genes (MRGs) may provide new insights into AML classification, prognosis, and therapeutic response.

Methods: We analyzed 72 MRGs using three independent AML datasets (TCGA-LAML, GSE24395, and GSE146173). Consensus clustering based on MRG expression was used to identify AML molecular subtypes. Differentially expressed genes (DEGs) common to AML subtypes and GSE24395 were identified. Prognostic genes were screened using univariate Cox regression and least absolute shrinkage and selection operator (Lasso) regression analyses. A prognostic risk model was constructed and validated. Functional enrichment, immune infiltration, and drug sensitivity analyses were conducted to explore the biological relevance of the model. In addition, regulatory elements including microRNAs, lncRNAs, and transcription factors targeting model genes were predicted.

Results: Twenty-six overlapping DEGs were identified between AML subtypes and GSE24395. Five MRG-associated genes (*ITGB2*, *VIP*, *PTK2*, *FHL2*, *BAG3*) were selected to construct a prognostic model that stratified patients into high- and low-risk groups with significantly different overall survival. Multivariate Cox analysis confirmed that risk score, age, and treatment status were independent prognostic indicators. Gene set enrichment analysis (GSEA) revealed 731 significantly enriched pathways, including mononuclear cell migration. Immune cell infiltration analysis showed a positive correlation between risk score and monocytes, and negative correlations with plasma B cells and activated mast cells. Drug sensitivity prediction identified 84 compounds with differential responses between risk groups. Regulatory network prediction highlighted hsa-miR-135b-5p, FTX, and SOX11 as potential upstream regulators of the prognostic genes.

Conclusion: This study identified five mitophagy-related genes as prognostic biomarkers in AML and developed a robust risk model that correlates with survival outcome, immune infiltration, and drug sensitivity. These findings offer new insights into mitophagy-related mechanisms in AML and may guide personalized therapeutic strategies.

KEYWORDS

acute myeloid leukemia, mitophagy-related genes, biomarkers, prognostic effect, immune infiltration

1 Introduction

Acute myeloid leukemia (AML), one of the most prevalent forms of acute leukemia in adults, is a malignant clonal disorder originating from hematopoietic stem cells (1). Characteristic features of AML include uncontrolled proliferation of leukemia stem cells (LSCs), impaired generation of functionally mature hematopoietic cells, bone marrow infiltration, and epigenetic dysregulation (2). The resultant suppression of normal erythrocyte, leukocyte, and platelet production leads to hallmark clinical symptoms such as hemorrhage, fever, and bone pain (3). In 2020, AML accounted for 2.5% of new cancer diagnoses and 3.1% of cancer-related deaths globally, ranking among the leading causes of cancer mortality (4). Prognosis remains poor, with some patients developing central nervous system involvement, further exacerbating disease severity and life-threatening complications (5). Standard therapy involves intensive induction chemotherapy followed by consolidation or allogeneic stem cell transplantation. Despite high initial response rates, relapse is common, and the 5-year survival rate remains at only 29.3% (6). Consequently, molecularly targeted therapies are garnering increasing attention. Small molecule inhibitors targeting key proteins and signaling pathways—such as FLT3, IDH, and BCL2—have shown clinical promise but often yield suboptimal and transient responses, contributing to therapeutic failure (7–9). Elucidating the molecular mechanisms underlying AML pathogenesis is therefore critical for advancing more effective treatment strategies.

Autophagy, a cellular degradation pathway, facilitates the removal of dysfunctional, damaged, or senescent cells, organelles, and proteins *via* lysosomal transport. Since the elucidation of its mechanism in 2016 (10), various autophagy subtypes—macroautophagy, chaperone-mediated autophagy, microautophagy, and selective autophagy—have garnered substantial research interest. Mitophagy, a mitochondria-specific form of autophagy, plays a pivotal role in maintaining mitochondrial quality control and cellular homeostasis while mitigating oxidative stress (11, 12). Hypoxia-induced mitophagy, mediated by receptors such as BNIP3, NIX, and FUNDC1, is notably upregulated under low-oxygen conditions (13). Both mitochondrial respiration and mitophagy are critically involved in the maintenance of LSCs (14–16). Experimental evidence indicates that disruption of mitochondrial homeostasis heightens the sensitivity of functional LSCs and hypoxic AML progenitors to autophagy inhibition (17). Moreover, elevated expression of the mitophagy receptor optineurin (OPTN) has been shown to suppress AML cell proliferation (18).

This study aims to investigate the role of mitophagy-related genes (MRGs) in the pathogenesis and progression of AML, offering valuable insights into early diagnosis and prognosis. A set of mitophagy-associated biomarkers was identified through integrated bioinformatics approaches, including differential gene expression analysis and machine learning, followed by the construction of a risk prediction model. Functional enrichment analysis, immune infiltration profiling, tumor mutational burden (TMB) assessment, and drug sensitivity evaluation were further conducted to elucidate the biological relevance and therapeutic

potential of these biomarkers. The findings provide a foundation for the development of more stable, efficacious, and safer therapeutic targets, offering novel clinical guidance for AML treatment.

2 Materials and methods

2.1 Data source

The AML-related dataset TCGA-LAML, comprising gene expression matrices and clinical data for 132 patients, was retrieved from the University of California, Santa Cruz (UCSC) Xena platform (<https://xenabrowser.net/datapages/>). Additionally, two gene expression profiles, GSE24395 (platform GPL610) and GSE146173 (platform GPL18460), were obtained from the Gene Expression Omnibus (GEO) database (<https://www.ncbi.nlm.nih.gov/gds>). The GSE24395 dataset contained 12 control and 5 AML patient samples, which were sequenced on the GPL6106 platform. Transcriptome raw counts were downloaded, and the mapping relationship between probe IDs and gene symbols was extracted according to the annotation file of the sequencing platform. The probe with the highest mean expression value for each gene symbol was retained, and data were processed using a 75th percentile shift normalization algorithm. The GSE146173 dataset included 202 AML patient samples, which were sequenced on the GPL18460 platform. After downloading the raw counts, ENSEMBL IDs were converted to gene symbols using the org.Hs.eg.db package (v 3.16.0) (19). Gene lengths were then obtained from the GPL18460 annotation file to calculate reads per kilobase (RPK). Further, fragments per kilobase of transcript per million mapped reads (FPKM) was computed, and \log_2 transformation ($\log_2^{(\text{FPKM} + 1)}$) was applied to the FPKM values to stabilize variance and facilitate subsequent analyses. Based on the October 16, 2023 version of the Kyoto Encyclopedia of Genes and Genomes (KEGG) human gene set (kegg_hsa.gmt), genes explicitly annotated to the “hsa04137_Mitophagy” pathway were screened. After removing duplicates, 72 mitophagy-related genes (MRGs) were obtained (Supplementary Table S1).

2.2 Consensus clustering analysis and differential expression analysis

To identify prognostically relevant MRGs, their expression profiles were extracted from the TCGA-LAML dataset and subjected to univariate Cox regression analysis ($P < 0.05$). Genes meeting this threshold were designated as prognostic MRGs. Using these genes, consensus clustering was performed on TCGA-LAML samples with the ConsensusClusterPlus package (v1.62.0) (20) to stratify molecular subtypes. The optimal number of clusters was determined based on the cumulative distribution function (CDF) curves and the delta area index. To assess survival differences among these subtypes, Kaplan-Meier (K-M) survival curves were constructed based on overall survival (OS) using the TCGA-LAML cohort. To further refine the analysis, differentially expressed genes

(DEGs) were identified in two comparisons: (1) between patients with AML and healthy controls in GSE24395 (denoted DEGs1), and (2) between the identified molecular subtypes within TCGA-LAML (denoted DEGs2). The limma (v1.38.0) and DESeq2 (v1.38.0) packages were applied for DEG analysis (21, 22), with thresholds of $|\log_2FC| > 1.5$ and adjusted P -value < 0.05 . The top 10 upregulated and downregulated genes from each comparison were visualized using volcano plots and heatmaps generated with the ggplot2 package (v3.4.1) (23).

2.3 Acquisition and functional enrichment analysis of candidate genes

Candidate genes were identified by intersecting DEGs1 and DEGs2. Functional interpretation of these candidates was conducted through Gene Ontology (GO) and KEGG pathway enrichment analyses using the clusterProfiler package (v4.7.1.3) (24), applying a significance cutoff of $P < 0.05$. Additionally, protein-protein interaction (PPI) networks for the candidate genes were constructed using the STRING database, with a minimum interaction confidence score set at 0.15.

2.4 Establishment and verification of risk model

The expression profiles of candidate genes in the TCGA-LAML dataset were first analyzed through univariate Cox regression ($P < 0.05$) to identify genes with prognostic significance. Subsequently, the least absolute shrinkage and selection operator (LASSO) regression was performed using the glmnet package (v4.1.4) to further refine the biomarker selection for constructing a prognostic risk model in the TCGA-LAML dataset (25).

A risk score was then computed for each patient with AML in the TCGA-LAML dataset based on the expression levels of selected biomarkers. Patients were stratified into high- and low-risk groups using the median risk score as a cutoff. Risk score distribution plots were generated to illustrate the separation between these two groups. K-M survival curves were constructed using the survminer package (v0.4.9) to evaluate differences in OS between the high- and low-risk cohorts (26). The predictive performance of the risk model was further assessed by time-dependent receiver operating characteristic (ROC) curves, plotted using the survivalROC package (27). In addition, the risk model was validated using risk scores, KM survival analysis, and ROC curve evaluation in the GSE146173 dataset. What's more, to further validate the reliability of a risk model as a clinical predictive tool for AML patients.

2.5 Independent prognostic analysis and nomogram construction

To assess the clinical utility of the model, TCGA-LAML samples were further categorized based on clinical variables

including age (≤ 60 / >60), gender (male/female), race (Asian/Black or African American/White), cytogenetic risk category (favorable/intermediate or normal/poor), treatment history (yes/no), and French-American-British (FAB) classification (M0–M7). Stratified K-M survival analyses were conducted for each subgroup using the survival package (v 3.5.3) (28). To identify independent prognostic indicators, both risk scores and clinical features were subjected to univariate Cox regression analysis. Variables meeting the significance threshold ($P < 0.05$) were subsequently tested for proportional hazards (PH) assumptions ($P > 0.05$) before inclusion in multivariate Cox regression, through which independent predictors of survival were identified.

A prognostic nomogram was then developed using the rms package based on the independently validated prognostic factors, allowing for the prediction of 1-, 3-, and 5-year OS in patients with AML (26). The predictive accuracy and calibration of the nomogram were validated using calibration plots generated with the rms package (v6.7.1) and time-dependent ROC curves plotted via the timeROC package (26, 29).

Finally, to investigate the relationship between risk stratification and clinical features, clinical annotations from TCGA-LAML were analyzed. Chi-square tests were used to assess statistical differences in clinical characteristics and survival outcomes between high- and low-risk groups (30).

2.6 Gene set enrichment analysis of different risk groups

In this study, differential gene expression analysis between high- and low-risk groups was conducted using the DESeq2 package (v1.38.0) (22). Genes were ranked by \log_2FC , sorted in descending order to prioritize those with the most significant expression differences. To elucidate the biological processes associated with these differences, GSEA was performed using the clusterProfiler package (v4.7.1.3) (24), referencing the GO Biological Process (GO-BP) category from the MSigDB database (c5.go.bp.v2023.1.Hs.symbols.gmt; <https://www.gsea-msigdb.org/>). Pathways meeting the criteria $|\text{normalized enrichment score (NES)}| > 1$ and $P < 0.05$ were considered significant, and the top five enriched pathways were selected for visualization.

2.7 Immune infiltration analysis

To characterize the immune landscape within the AML samples from the TCGA-LAML dataset, the CIBERSORT algorithm was applied to estimate the relative abundance of 22 immune cell types (31). Differences in immune cell infiltration between risk groups were evaluated using the Wilcoxon signed-rank test ($P < 0.05$). Additionally, Spearman correlation analysis was employed to explore associations between immune cell proportions and risk scores, with results considered significant when $|r| > 0.4$ and $P < 0.05$. Immune checkpoint gene expression analysis was also performed by extracting the expression levels of eight key

immune regulatory genes—CD274, LAG3, TGFBI, TNFSF13, CD4, CD40, CD80, and CD276—from the TCGA-LAML dataset. Group-wise comparisons of these genes were conducted using the Wilcoxon test ($P < 0.05$), and their correlation with risk scores was visualized *via* scatter plots. To further elucidate the interaction between key biomarkers and the tumor immune microenvironment, relevant immune cell reporter genes and immune regulatory genes were retrieved from the TISIDB database (<http://cis.hku.hk/TISIDB/>). Spearman correlation analysis was then conducted between selected biomarkers and these immune-related genes, with $|r| > 0.4$ and $P < 0.05$ indicating statistically significant associations.

2.8 Drug sensitivity analysis

To explore the association between biomarkers and chemotherapeutic response, half-maximal inhibitory concentration (IC_{50}) values for 138 commonly used chemotherapeutic agents were estimated using the pRRophetic package (v0.5) (32) across all TCGA-LAML samples, followed by comparative analysis between risk groups. In addition, the corrplot package (v 0.92) (33) was used to evaluate the correlations between the top 20 drugs with significant differences in IC_{50} between the high-risk and low-risk groups and the 5 biomarkers through Spearman correlation analysis ($|r| > 0.4$ and $P < 0.05$).

2.9 Molecular regulatory network construction

To elucidate potential regulatory mechanisms of the identified biomarkers in AML, upstream elements were predicted. miRNAs targeting the biomarkers were identified *via* miRDB (<https://mirdb.org/>) and miRanda (<http://www.microrna.org/microrna/home.do>). miRNAs common to both databases were then used to predict interacting long non-coding RNAs (lncRNAs) through the starBase platform (<http://starbase.sysu.edu.cn/>). Transcription factors (TFs) potentially regulating the biomarkers were inferred from the ChEA3 database (<https://maayanlab.cloud/chea3>). The lncRNA-miRNA-mRNA and mRNA-TF regulatory networks were visualized using Cytoscape (v3.10.2).

2.10 Validation of biomarker expression

Expression levels of the biomarkers were examined in the GSE24395 dataset, with statistical significance defined at $P < 0.05$. Validation of biomarker expression was further conducted *via* quantitative reverse transcription PCR (qRT-PCR). Whole blood samples from fifteen patients with AML and fifteen healthy donors, collected at the Second Hospital of Hebei Medical University, were used for qRT-PCR analysis. All participants provided written informed consent, and the study was approved by the institutional ethics committee.

Total RNA was extracted from frozen samples using TRIzol reagent (Ambion, China). Equal amounts of mRNA were

reverse-transcribed to synthesize cDNA. qPCR was conducted using the 2 × Universal Blue SYBR Green qPCR Master Mix kit (Servicebio, China), following standard protocols. Gene expression levels were quantified using the $2^{-\Delta\Delta CT}$ method. Primer sequences are listed in Supplementary Table S2.

2.11 Statistical analysis

All bioinformatics analyses were performed using R software (v4.2.2), with $P < 0.05$ considered statistically significant.

3 Results

3.1 Consensus clustering analysis among patients with AML

Expression profiling of 72 MRGs in the TCGA-LAML dataset identified 15 prognostic MRGs through univariate Cox regression analysis, which were subsequently used for consensus clustering (Figure 1a). Based on the CDF curves and delta area index, the optimal number of clusters was determined as $k=2$, and the samples in the TCGA-LAML dataset were divided into two subtypes, namely subtype 1 and subtype 2 (Figure 1b)—with their distribution visualized *via* t-SNE dimensionality reduction (Figure 1c). K-M survival analysis revealed a statistically significant difference in OS between the subtypes, with subtype 1 associated with a poorer prognosis (Figure 1d).

3.2 A total of 26 genes were identified as candidate genes

Differential expression analysis was conducted to identify disease- and subtype-specific transcriptomic alterations. A total of 294 DEGs1, including 223 upregulated and 71 downregulated genes, were identified between AML samples and controls in the GSE24395 dataset (Figures 2a, b). In parallel, a total of 819 DEGs2 (205 upregulated and 614 downregulated) were identified between subtype 1 and subtype 2 in the TCGA-LAML dataset (Figures 2c, d). The intersection of DEGs1 and DEGs2 yielded 26 candidate genes for further analysis (Figure 2e, Supplementary Table S3). These 26 genes were subjected to functional enrichment analysis. GO analysis revealed enrichment in 348 terms, comprising 277 biological processes (BPs), 36 cellular components (CCs), and 35 molecular functions (MFs). The top five enriched terms were predominantly related to neutrophil activation, focal adhesion, and phosphoric diester hydrolase activity, among others (Figure 2f). KEGG pathway analysis identified 15 significantly enriched signaling pathways, with the top five including regulation of the actin cytoskeleton and rheumatoid arthritis (Figure 2g). Furthermore, PPI network analysis highlighted 24 interacting genes, forming key interaction axes such as *PTK2-ITGB2*, *PTK2-BAG3*, and *BAG3-FHL2* (Figure 2h).

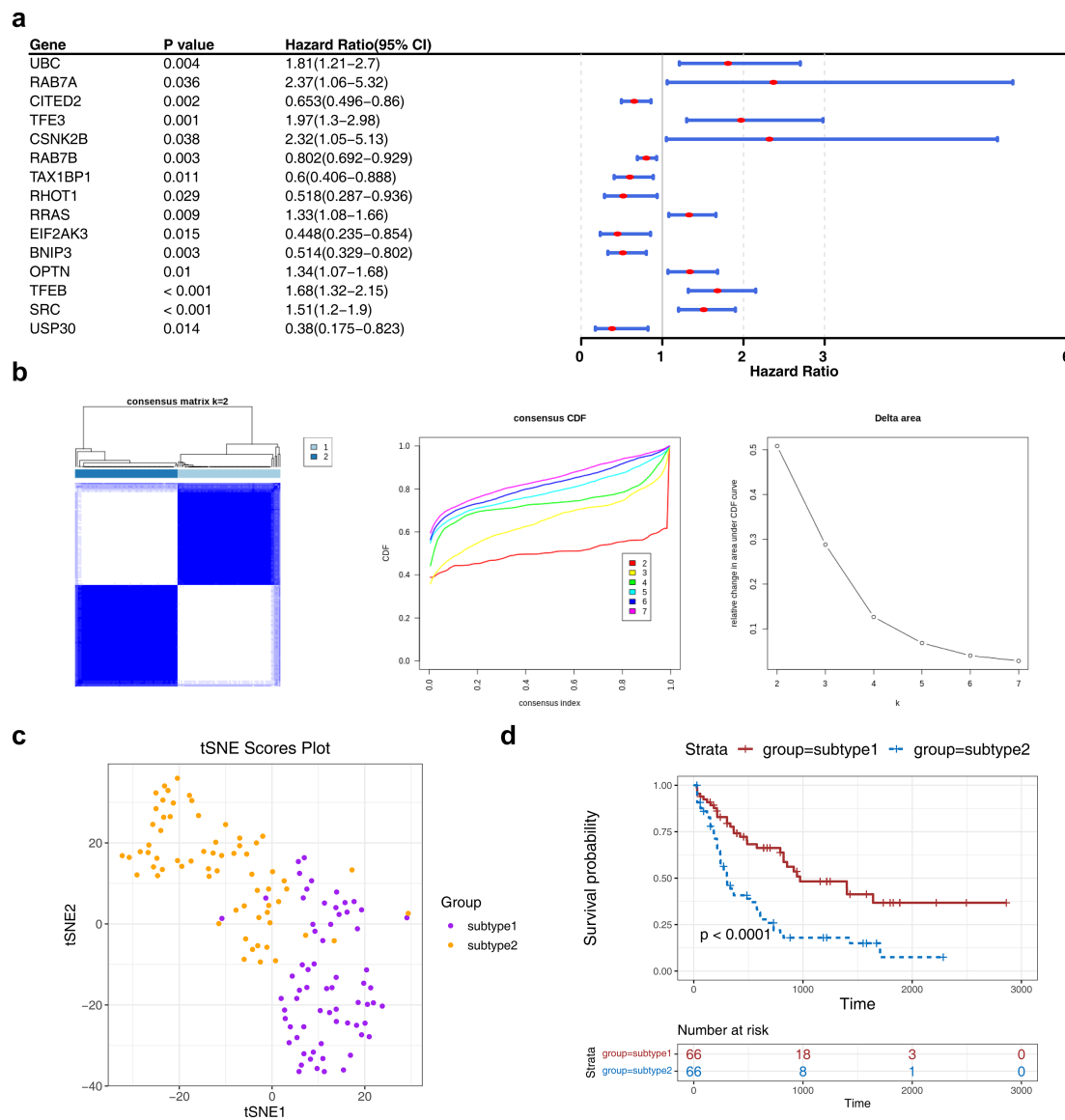


FIGURE 1

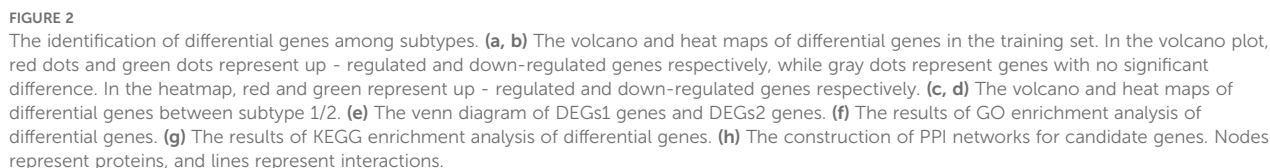
The consensus clustering analysis among AML patients. (a) The forest plot of MRG associated with prognosis in AML patients. The figure showed the names of MRGs, P-values, HR values, and 95% CIs. An HR value greater than 1 was indicated to be a risk factor for AML, while an HR value less than 1 was indicated to be a protective factor. (b, c) The consensus cluster analysis of prognosis-related MRGs in AML patients. AML patients were classified into two subtypes based on MRGs. (d) The K-M curve of different subtypes. Red represents subtype 2, and blue represents subtype 1.

3.3 *ITGB2*, *VIP*, *PTK2*, *FHL2*, and *BAG3* were identified as biomarkers for constructing risk models

Lasso regression analysis was conducted on six genes (*ITGB2*, *VIP*, *PTK2*, *FHL2*, *BAG3*, *EPB41L3*) previously identified via univariate Cox regression (Figure 3a). The analysis retained five genes—*ITGB2*, *VIP*, *PTK2*, *FHL2*, and *BAG3*—with non-zero regression coefficients, which were subsequently selected as biomarkers for constructing the prognostic risk model (Figures 3b, c). The risk score was calculated using the following formula: Risk score = $0.22405735 \times ITGB2$ expression + $0.07079774 \times VIP$ expression + $0.03667777 \times PTK2$ expression + $0.12551123 \times$

FHL2 expression + $0.19284549 \times BAG3$ expression. Based on the median risk score, patients with AML were stratified into high- and low-risk groups (n = 66 per group). A clear positive association between risk score and mortality was observed (Figures 3d, e). K-M survival analysis demonstrated significantly reduced OS in the high-risk group (Figure 3f). ROC curve analysis revealed areas under the curve (AUCs) of 0.71, 0.69, and 0.77 for 1-, 3-, and 5-year survival, respectively, indicating robust predictive performance of the model (Figure 3g).

The model's predictive validity was externally verified using the GSE146173 dataset. Similar trends were observed, with high-risk patients exhibiting reduced survival (Supplementary Figures S1a–c). AUC values consistently exceeded 0.6, aligning well with results



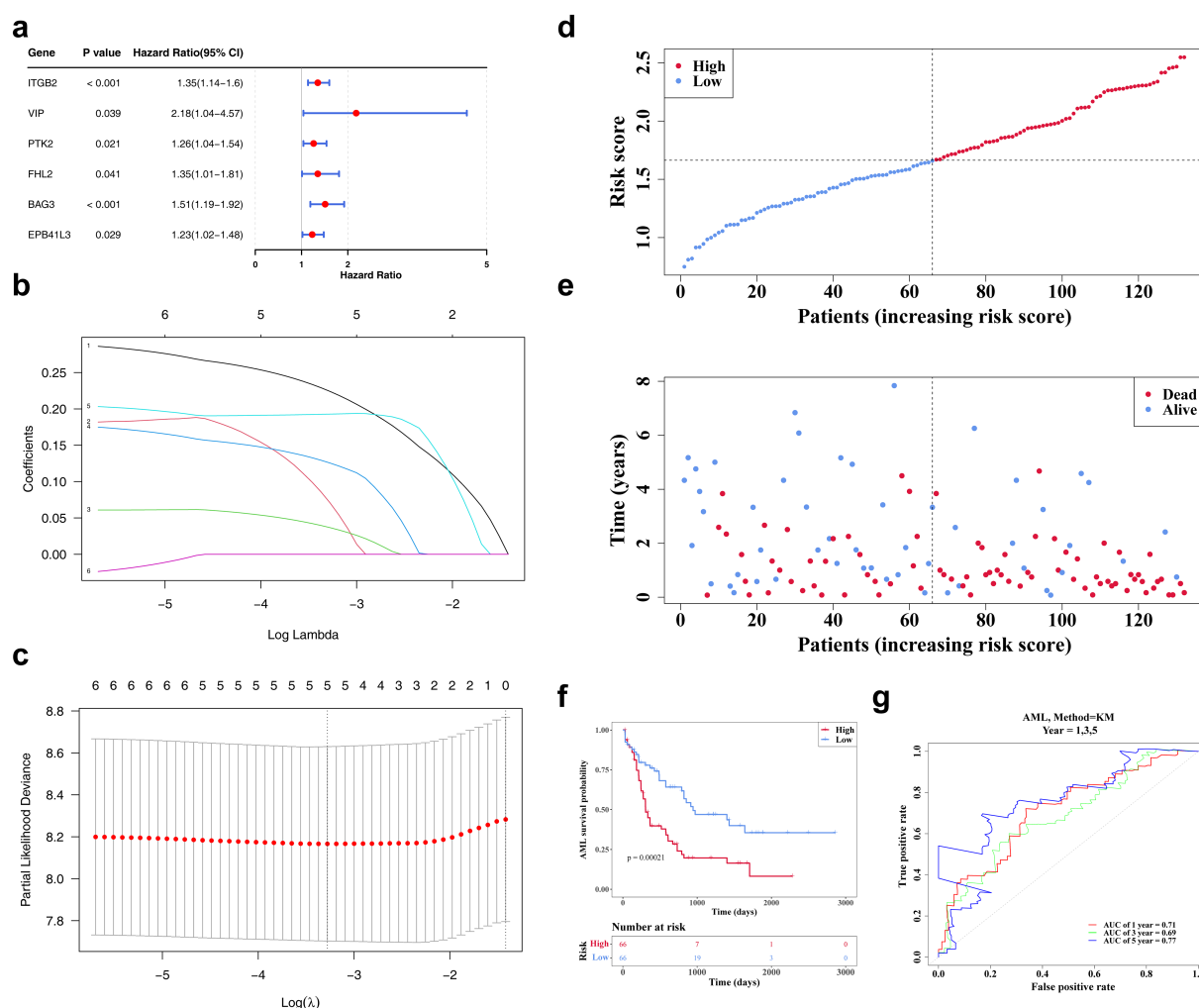


FIGURE 3

The identification of biomarkers. **(a)** The forest map of prognosis-related candidate genes. It shows the P-values, HR, and 95% CIs for multiple genes, which are used to evaluate the impact of each gene on AML risk. **(b, c)** The LASSO regression coefficient graph and cross-validation graph based on penalty term. **(d)** The risk curves of the TCGA-LAML sample. The red line represents the high-risk group, and the blue line represents the low-risk group. **(e)** The survival status distributions for the TCGA-LAML sample. Red dots represent deceased patients, while blue dots represent surviving patients. **(f)** The TCGA-AML K-M curves for high and low risk groups. Red represents the high-risk group, and blue represents the low-risk group. **(g)** The ROC curve of the model in TCGA-AML. An AUC value greater than 0.6 indicates that the model has certain predictive performance.

from the TCGA-LAML cohort (Supplementary Figure S1d), confirming the model's reliability and generalizability as a clinical prognostic tool for AML.

3.4 The risk score, age, and treatment were independent prognostic factors for AML

Analysis of clinical parameters revealed that age, health status, treatment regimen, and FAB classification significantly influenced the outcomes of patients with AML. In particular, patients aged ≤ 60 years, with favorable health, no prior treatment, or FAB classification M3, showed markedly improved survival (Supplementary Figures S2a–f). Univariate Cox regression analysis confirmed the prognostic significance of risk score, age, health status, and treatment, with consistency across PH assumption testing (Figure 4a).

Multivariate Cox regression further identified risk score, age, and treatment as independent prognostic factors (Figure 4b). A prognostic nomogram incorporating these independent variables was developed to estimate individualized survival probabilities for patients with AML (Figure 4c). The calibration curve demonstrated strong concordance between predicted and observed survival outcomes (Figure 4d). ROC curve analysis of the nomogram yielded AUC values exceeding 0.6 at 1, 3, and 5 years, supporting its high predictive accuracy (Figure 4e).

Comparative analysis of clinical characteristics between high- and low-risk groups indicated significant differences in age, health status, FAB classification, and OS (Supplementary Figure S3a). Additionally, GSEA identified 731 significantly enriched functional terms between risk groups, with the top five—including mononuclear cell migration and cellular response to biotic stimulus—highlighted in the visualization (Supplementary Figure S3b).

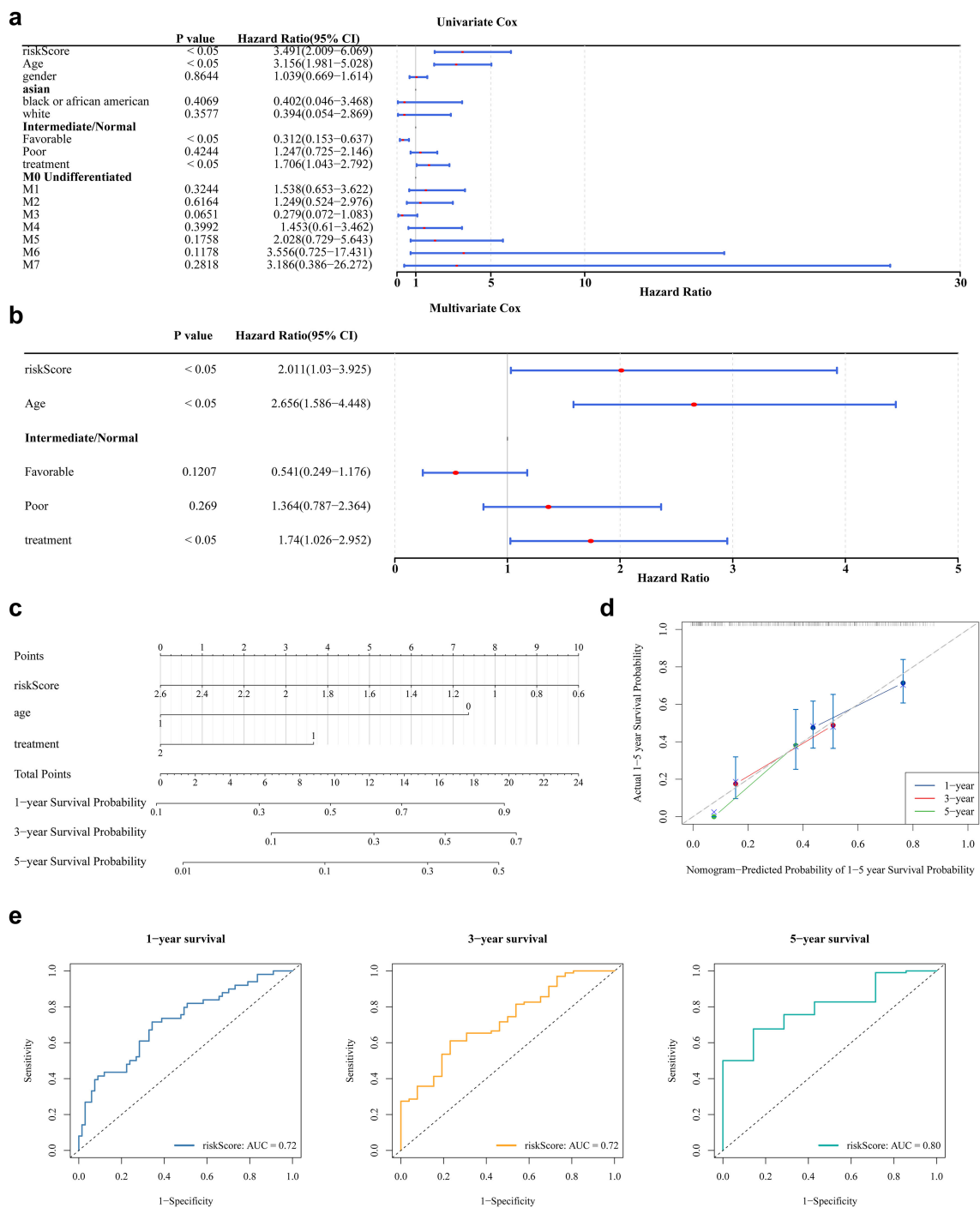


FIGURE 4 Nomogram model construction and evaluation. **(a)** The results of univariate Cox analysis. It shows the P-values, HR values, and 95% CI values for different variables. **(b)** The results of multivariate Cox regression analysis. **(c)** The construction of nomogram. In the variable “age”, values greater than 65 years are coded as 1, and those less than 65 years are coded as 0. In the variable “treatment”, patients who received treatment are coded as 2, while those who did not receive treatment are coded as 1. In the “risk score”, the values ranging from 2.6 to 0.6 correspond to the risk values of the samples. Each variable is assigned a score, and the total score is calculated based on the scores of all variables to predict the 1-year, 3-year, and 5-year survival probabilities of AML. **(d)** The calibration curve showed that the accuracy of the nomogram was relatively high and validated the model performance of AML. **(e)** The ROC curve indicates that the nomogram model has an excellent predictive value for AML (AUC>0.6).

3.5 Seven immune cells differed significantly by risk group

Immune cell infiltration was assessed using the CIBERSORT algorithm, which estimated the relative abundance of 22 immune cell types (Figure 5a). Significant differences in immune infiltration were observed between risk groups for seven cell types. Specifically, five immune cells—naïve B cells, plasma B cells, eosinophils, activated mast cells, and memory-resting CD4⁺ T cells—exhibited significantly reduced infiltration in the high-risk group. In contrast, monocytes and memory-activated CD4⁺ T cells showed no significant decline (Figure 5b). Correlation analysis revealed a strong positive association between monocyte infiltration and risk scores ($r > 0.4$, $P < 0.05$), while plasma B cells and activated mast cells were negatively correlated with risk scores ($r < -0.4$, $P < 0.05$) (Figure 5c). Among eight examined immune checkpoints, seven (CD274, LAG3, TIGIT, TNFSF13, CD4, CD40, and CD276) were significantly overexpressed in the high-risk group, with CD80 as the only exception (Figure 5d). Risk scores exhibited positive correlations with the expression levels of all eight immune checkpoints (Figure 5e). Additionally, a total of 315 cell reporter genes and 65 immune regulatory genes showed significant associations with the biomarkers, as depicted in heatmaps (Figures 5f, g).

3.6 A total of 84 drugs were sensitive to AML

Drug sensitivity analysis identified 84 compounds with significantly different IC50 values between the two risk groups. Notable examples included AS601245, BIBW2992, and Bleomycin (Supplementary Figures S4a, b), suggesting distinct therapeutic vulnerabilities associated with molecular risk stratification. Furthermore, AS601245, BIBW2992, and Bleomycin all showed strong negative correlations with the 5 biomarkers ($r < -0.3$) (Supplementary Figure S4c).

3.7 Various regulatory elements of *ITGB2*, *VIP*, *PTK2*, *FHL2* and *BAG3*

Regulatory elements of *ITGB2*, *VIP*, *PTK2*, *FHL2*, and *BAG3* were systematically predicted. The constructed lncRNA–miRNA–mRNA regulatory network included miRNAs such as hsa-miR-135b-5p, hsa-miR-452-5p, and hsa-miR-543, which target the biomarkers, and upstream lncRNAs including FTX, HCG11, and PURPL that regulate these miRNAs (Figure 6a). TFs were also predicted: SOX11 targeting *ITGB2* and *PTK2*, TLX2 regulating *VIP*, AKAP8L acting on *FHL2*, and SIX2 targeting *BAG3* (Figure 6b). These regulatory elements are critical for elucidating the mechanistic roles of MRGs in AML progression.

3.8 The expression of biomarkers

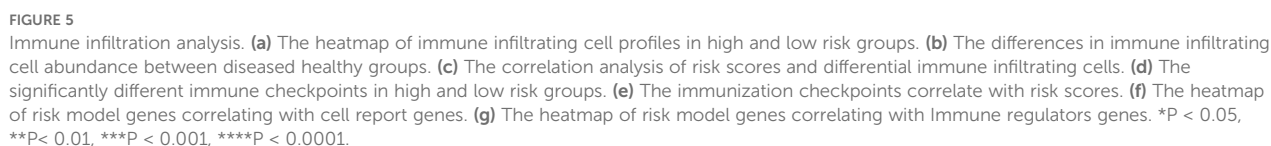
Expression validation using the GSE24395 dataset indicated significant downregulation of *VIP*, *PTK2*, *FHL2*, and *BAG3* in AML samples, while *ITGB2* was upregulated (Figure 7a). These findings were further corroborated by qRT-PCR, which confirmed reduced expression of *PTK2*, *FHL2*, *VIP*, and *BAG3*, and elevated expression of *ITGB2* in AML samples (Figure 7b).

4 Discussion

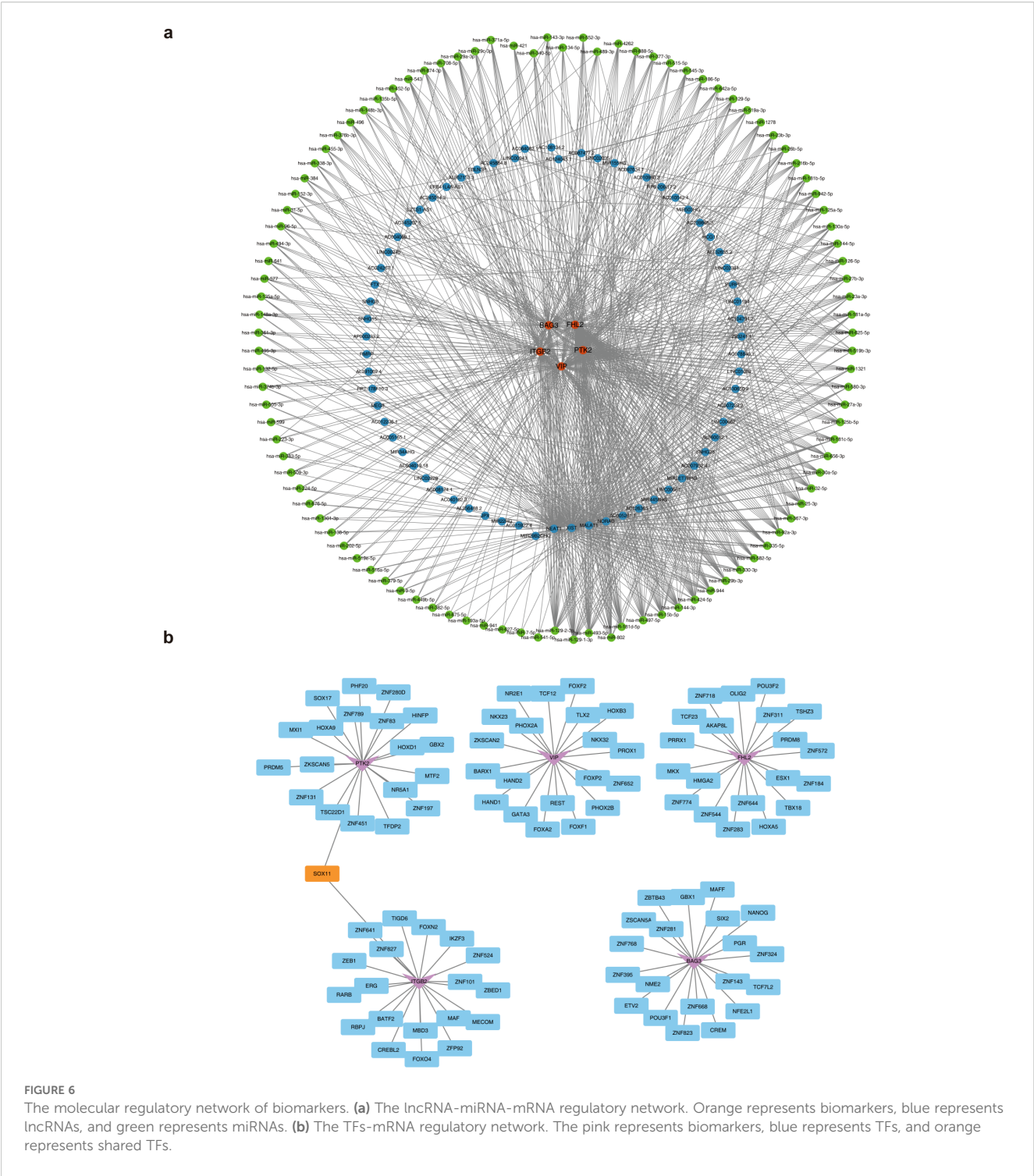
AML, a group of highly heterogeneous hematologic malignancies, is characterized by poor therapeutic outcomes and short survival durations, particularly among patients with intermediate- to high-risk disease or refractory/relapsed forms. This clinical challenge underscores an urgent need to expand therapeutic strategies for AML. Although the role of mitophagy and mitochondrial homeostasis in cancer has been increasingly recognized (34–36), including the established function of SQSTM1 in leukemia progression (14), the specific mechanisms by which MRGs drive AML heterogeneity remain incompletely defined.

In this study, we conducted univariate Cox regression analysis to screen 15 prognostically related MRGs for concordance cluster analysis. Ultimately, AML patients were divided into two distinct subtypes, namely subtype 1 and subtype 2. Cluster analysis based on MRGs uncovered significant molecular heterogeneity within the AML patient population (37). The marked survival differences between the subtypes imply potential discrepancies in sensitivity to existing treatments. This suggests that clinicians could personalize treatment strategies according to the subtype-specific characteristics (38). The lower survival rates observed in subtype 1 patients indicate that this subtype might be associated with a more active aberrant mitophagy process or accompanied by other molecular events linked to poor prognosis. These abnormalities may contribute to the unfavorable prognosis of subtype 1 patients by potentially accelerating leukemia cell proliferation, inducing drug resistance, or facilitating immune surveillance evasion (18, 39). Furthermore, subtype classification can aid in patient stratification during clinical trials, thereby enhancing the accuracy and effectiveness of novel therapy evaluation (40).

In this study, 26 candidate genes were obtained by intersection analysis of 294 DEGs1 from between AML and control groups and 819 DEGs2 from between different subtypes. Subsequent univariate Cox and Lasso regression analyses identified five key biomarkers—*ITGB2*, *VIP*, *PTK2*, *FHL2*, and *BAG3*—for constructing a prognostic risk model. Among them, *ITGB2*, encoding the CD18 integrin subunit, was initially identified in leukocytes, where it mediates adhesion to endothelial cells and facilitates transendothelial migration. Prior research has implicated *ITGB2* in drug resistance mechanisms to mitoxantrone and idarubicin in



prognosis. Mechanistically, ITGB2 may influence mitophagy through its role in cell adhesion and stress response signaling. Studies suggest that integrin-mediated adhesion pathways can modulate mitochondrial homeostasis under cellular stress,



potentially linking ITGB2 to dysregulated mitophagy in AML progression. *VIP* (vasoactive intestinal peptide), a 28-amino acid neuropeptide initially isolated from porcine duodenum, is widely distributed across multiple physiological systems including the nervous, reproductive, and respiratory systems (44). Although *VIP* has been shown to mitigate bleomycin-induced pulmonary fibrosis by restoring autophagy in alveolar epithelial cells (45), its role in hematologic malignancies remains unexplored. Notably, *VIP* may regulate mitochondrial function via the cAMP/PKA pathway,

which is implicated in coordinating energy metabolism and mitophagy. This pathway could contribute to mitochondrial quality control in leukemia cells, offering a potential mechanistic link between *VIP* and mitophagy in AML (46–48). *PTK2* (protein tyrosine kinase 2), also known as focal adhesion kinase (FAK), functions as a non-receptor tyrosine kinase regulating integrin and growth factor receptor signaling (49). Elevated expression of *PTK2* has been documented in various malignancies such as lung cancer, hepatocellular carcinoma, and lymphocytic leukemia (50, 51).

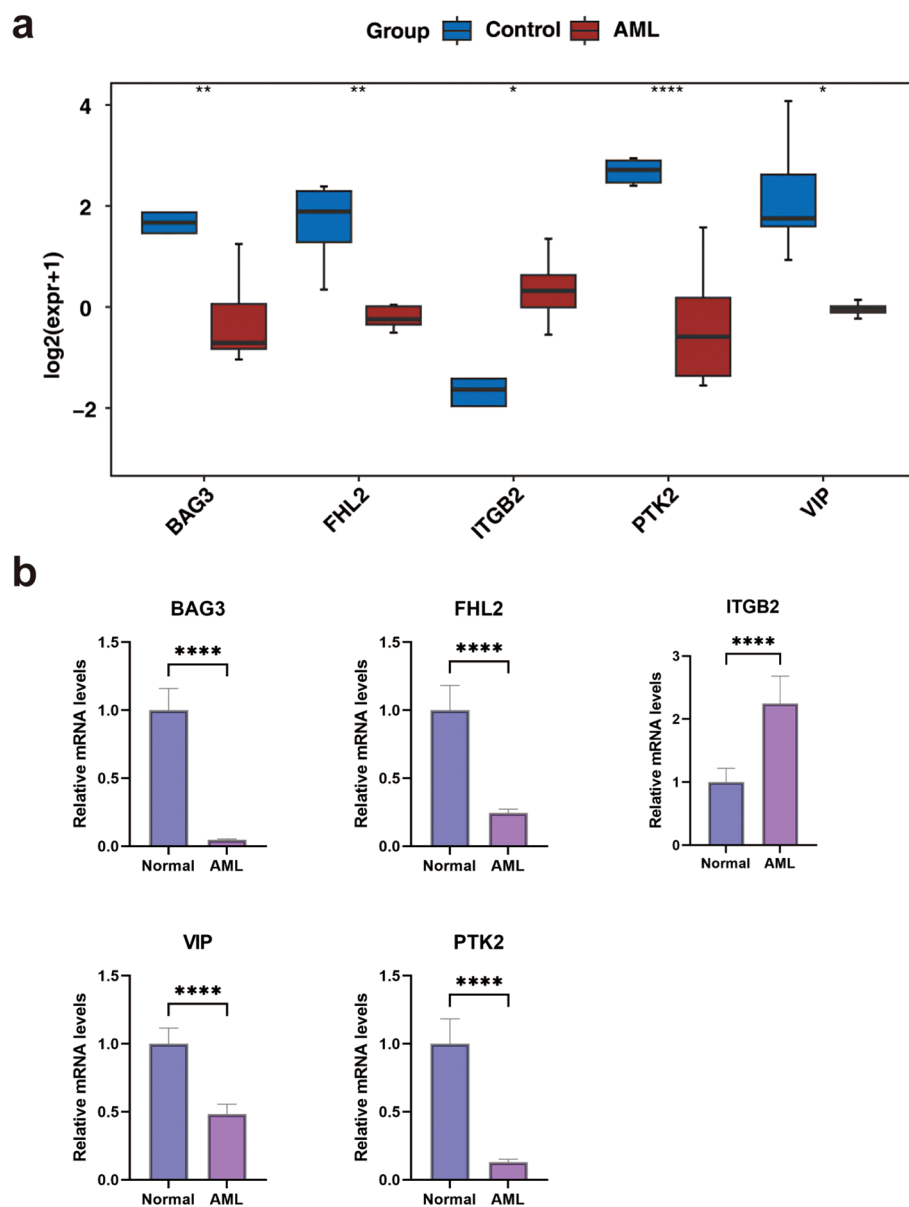


FIGURE 7

The expression levels of biomarkers. (a) In the GSE24395 dataset, the expression levels of biomarkers between AML and control groups. (b) The qRT-PCR of biomarkers. * $P < 0.05$, ** $P < 0.01$, *** $P < 0.001$, **** $P < 0.0001$.

Furthermore, *PTK2* has been identified as an independent prognostic factor in AML, particularly in intermediate-risk cohorts. *PTK2* may further influence mitophagy through its modulation of mitochondrial membrane potential and ROS production. Crosstalk between focal adhesion kinase signaling and autophagy pathways could disrupt mitochondrial quality control, promoting survival of leukemic stem cells (52–54). It also serves as a prognostic discriminator among patients harboring unfavorable *FLT3*/*NPM1* mutations with concurrent low *PTK2B* or *LYN* expression (55). The *FHL2* protein is localized in adhesion plaques, the cytoplasm, and the nucleus, where it interacts with a broad array of TFs and tumor-associated proteins (56, 57). Its expression is markedly elevated in gastric cancer tissues compared

to chronic gastritis, with overexpression closely linked to gastric tumorigenesis (58). Emerging evidence also implicates *FHL2* in leukemogenesis (59). Beyond its oncogenic potential, *FHL2* plays a pivotal role in regulating the survival of hematopoietic stem cells under both homeostatic and stress conditions. While not directly linked to mitophagy, this role in mitochondrial dynamics provides a novel angle to explore its contribution to mitophagic flux in AML (60). *BAG3* (Bcl-2-associated athanogene 3), a member of the BAG protein family, exerts its biological functions by interacting with target proteins *via* multiple structural motifs, including the BAG domain, WW domain, and PXXP motif. It is involved in a range of cellular processes such as autophagy, apoptosis, embryogenesis, cytoskeletal reorganization, and cell migration (61, 62). *BAG3* is

aberrantly expressed in several solid tumors and germ cell leukemias (62, 63), and has been proposed as a potential therapeutic target in cancers including glioma, pancreatic cancer, and ovarian carcinoma. Additionally, BAG3 is upregulated in response to various cellular stressors, facilitating selective autophagy to maintain intracellular homeostasis (64–68). As a co-chaperone, BAG3 directly interacts with HSP70 via its BAG domain to facilitate selective autophagy of damaged organelles, including mitochondria (69, 70). This HSP70-BAG3 complex recruits LC3 to ubiquitinated substrates, positioning BAG3 as a critical regulator of mitophagic clearance in cancer cells (71). Its overexpression may thus confer a survival advantage to AML blasts by enhancing mitochondrial turnover. In summary, five biomarkers—*ITGB2*, *VIP*, *PTK2*, *FHL2*, and *BAG3*—were identified in this study as being associated with AML. These genes appear to be functionally relevant to AML pathogenesis and may serve as valuable molecular targets for future diagnostic and therapeutic strategies.

The results of this study showed that in the TCGA-LAML data set, the risk score was significantly positively correlated with patient mortality. The difference in survival between high- and low-risk groups was statistically significant, and the 5-year ROC curve AUC value was 0.77. These results are highly consistent with the range of performance of AML prognostic models reported in previous studies (72). Furthermore, the consistency between the results and the external validation set (GSE146173) fully reflects the reliability and universality of the model in predicting long-term prognosis. Additionally, from the association analysis of clinical characteristics and prognosis, patients aged ≤ 60 years, in good health, untreated, or FAB-typed as M3 had a significantly higher survival rate. This finding is consistent with the clinical perception that younger patients are in better physical condition and that M3 AML patients are sensitive to targeted therapies (73). The nomogram model integrates independent prognostic factors such as risk score, age, and treatment type. Its predictive accuracy was verified by calibration curve and ROC analysis, providing a visual decision-making tool for clinical practice (74). For example, in elderly patients with a high-risk score and comorbidities, the model may suggest a poor prognosis and the need to prioritize intensive supportive care or novel therapies (75). Younger patients with a lower risk score may benefit more from standard care (76). GSEA enrichment results in high- and low-risk groups (monocyte migration, biostimulatory response pathways) revealed that the risk model may be associated with immune microenvironment heterogeneity or abnormal regulation of inflammation in AML (77). The activation of monocyte migration-related pathways may be associated with leukemia cell infiltration or immune escape mechanisms. This provides directions for further exploration of AML pathogenesis and the development of therapeutic strategies targeting immune checkpoints or inflammatory signaling pathways (78).

Immunotherapy based on immune checkpoint inhibitors (ICIs) has garnered increasing attention for its efficacy in treating advanced, metastatic, and recurrent malignancies. By disrupting inhibitory checkpoint signaling, ICIs restore anti-tumor immune

responses. Clinical success has been demonstrated in cancers such as melanoma, lung, and prostate cancer (79–82). APRIL/TNFSF13, an immune checkpoint molecule, is overexpressed in colorectal and glioma tissues and has been linked to adverse pathological features and poor prognosis, suggesting its potential as a therapeutic target (83, 84). In addition, the therapeutic relevance of tumor-infiltrating B cells has been established in colorectal cancer (85).

Although immune checkpoint and immune infiltration analyses have significantly contributed to predictive modeling and drug sensitivity profiling in solid tumors, similar investigations in AML remain limited. The present analysis highlights monocytes, plasma B cells, and activated mast cells as key immune populations associated with risk stratification in AML. Moreover, targeting immune checkpoints such as TGFBI, TNFSF13, CD4, and CD40 may enhance immunotherapeutic efficacy in AML. Nonetheless, further mechanistic studies are required to elucidate the specific roles of these immune cells and immune checkpoints within the AML microenvironment.

Accumulating evidence highlights the pivotal role of mitophagy in the pathogenesis of AML, with its modulation offering potential to enhance therapeutic efficacy and overcome drug resistance. Elucidating specific molecular mechanisms and identifying precise regulatory targets thus represent promising strategies for advancing AML treatment. In the present study, MRGs were associated with AML through differential expression analysis, consensus clustering, univariate Cox regression, LASSO modeling, and related computational approaches. Five prognostic biomarkers were identified and incorporated into a risk prediction model, providing a theoretical framework for further exploration of MRGs in AML. Nevertheless, the clinical utility of these biomarkers remains constrained by limited sample size, and additional mechanistic studies and larger cohorts are essential to validate their translational potential in AML therapy.

Although this study used bioinformatics to screen five mitophagy genes linked to AML prognosis and built a risk model, several limitations exist. Existing research has predominantly utilized data from public databases such as TCGA and GEO. There is a lack of experimental validation regarding the specific functions of these biomarkers in AML. Despite MRGs being effective in patient stratification within both the TCGA and GSE146173 datasets, smaller datasets like GSE24395 may suffer from insufficient statistical power. In the future, CRISPR-Cas9 technology can be used to manipulate target genes in AML cell lines. By combining this with assays such as CCK-8, mitochondrial membrane potential detection, and autophagic flux analysis, we can clarify how these genes regulate mitophagy pathways and cellular phenotypes. The *in vivo* functionality can be verified using AML mouse models. Furthermore, ChIP-seq and proteomics technologies can be utilized to analyze the regulatory network of these biomarkers within the context of AML cell heterogeneity and the immune microenvironment. This analysis can provide theoretical support for developing novel therapies that target mitophagy pathways.

5 Conclusion

Five prognostic biomarkers—*ITGB2*, *VIP*, *PTK2*, *FHL2*, and *BAG3*—were identified and integrated into a novel risk model to stratify patients with AML into high- and low-risk groups. This classification revealed distinct molecular and immunological profiles between the two groups, as demonstrated by differences in functional enrichment patterns, immune cell infiltration, somatic mutation landscapes, and drug sensitivity. The findings offer a set of clinically relevant biomarkers with prognostic and therapeutic significance, providing new insights into personalized treatment strategies and disease management in AML.

Data availability statement

The original contributions presented in the study are included in the article/**Supplementary Files**, further inquiries can be directed to the corresponding author/s.

Ethics statement

The studies involving humans were approved by Research Ethics Committee of the Second Hospital of Hebei Medical University. The studies were conducted in accordance with the local legislation and institutional requirements. Written informed consent for participation in this study was provided by the participants' legal guardians/next of kin.

Author contributions

FX: Conceptualization, Data curation, Validation, Visualization, Writing – original draft, Writing – review & editing. WZ: Data curation, Validation, Visualization, Writing – review & editing. BZ: Validation, Writing – review & editing. HZ: Visualization, Writing – review & editing. CL: Conceptualization, Supervision, Writing – review & editing. XW: Conceptualization, Project administration, Supervision, Writing – review & editing.

Funding

The author(s) declare financial support was received for the research and/or publication of this article. The research reported in

this project was generously supported by Hebei Natural Science Foundation Hebei Provincial Health Commission under grant agreement number H2020206301, H2023206222 and 20230524. The funders had no role in study design, data collection and analysis, decision to publish, or preparation of the manuscript.

Acknowledgments

We would like to express our sincere gratitude to all individuals and organizations who supported and assisted us throughout this research. Special thanks to the following authors: In conclusion, we extend our thanks to everyone who has supported and assisted us along the way. Without your support, this research would not have been possible.

Conflict of interest

The authors declare that the research was conducted in the absence of any commercial or financial relationships that could be construed as a potential conflict of interest.

Generative AI statement

The author(s) declare that no Generative AI was used in the creation of this manuscript.

Publisher's note

All claims expressed in this article are solely those of the authors and do not necessarily represent those of their affiliated organizations, or those of the publisher, the editors and the reviewers. Any product that may be evaluated in this article, or claim that may be made by its manufacturer, is not guaranteed or endorsed by the publisher.

Supplementary material

The Supplementary Material for this article can be found online at: <https://www.frontiersin.org/articles/10.3389/fimmu.2025.1580597/full#supplementary-material>

References

1. Bednarczyk M, Kociszewska K, Grosicka O, Grosicki S. The role of autophagy in acute myeloid leukemia development. *Expert Rev Anticancer Ther.* (2023) 23:5–18. doi: 10.1080/14737140.2023.2161518
2. Short NJ, Konopleva M, Kadia TM, Borthakur G, Ravandi F, DiNardo CD, et al. Advances in the treatment of acute myeloid leukemia: new drugs and new challenges. *Cancer Discov.* (2020) 10:506–25. doi: 10.1158/2159-8290.CD-19-1011
3. Hasserjian RP, Steensma DP, Graubert TA, Ebert BL. Clonal hematopoiesis and measurable residual disease assessment in acute myeloid leukemia. *Blood.* (2020) 135:1729–38. doi: 10.1182/blood.2019004770
4. Sung H, Ferlay J, Siegel RL, Laversanne M, Soerjomataram I, Jemal A, et al. Global cancer statistics 2020: GLOBOCAN estimates of incidence and mortality worldwide for 36 cancers in 185 countries. *CA Cancer J Clin.* (2021) 71:209–49. doi: 10.3322/caac.21660

5. Saad M, Loh KP, Tooze JA, Pardee TS, Ellis LR, Powell BL, et al. Geriatric assessment and survival among older adults receiving postremission therapy for acute myeloid leukemia. *Blood*. (2020) 136:2715–9. doi: 10.1182/blood.2020005498
6. Hackl H, Astanina K, Wieser R. Molecular and genetic alterations associated with therapy resistance and relapse of acute myeloid leukemia. *J Hematol Oncol*. (2017) 10:51. doi: 10.1186/s13045-017-0416-0
7. Antar AI, Otrrock ZK, Jabbour E, Mohty M, Bazarbachi A. FLT3 inhibitors in acute myeloid leukemia: ten frequently asked questions. *Leukemia*. (2020) 34:682–96. doi: 10.1038/s41375-019-0694-3
8. Liu X, Gong Y. Isocitrate dehydrogenase inhibitors in acute myeloid leukemia. *biomark Res*. (2019) 7:22. doi: 10.1186/s40364-019-0173-z
9. Konopleva M, Letai A. BCL-2 inhibition in AML: an unexpected bonus? *Blood*. (2018) 132:1007–12. doi: 10.1182/blood-2018-03-828269
10. Tooze SA, Dikic I. Autophagy captures the nobel prize. *Cell*. (2016) 167:1433–5. doi: 10.1016/j.cell.2016.11.023
11. Palikaras K, Tavernarakis N. Mitochondrial homeostasis: the interplay between mitophagy and mitochondrial biogenesis. *Exp Gerontol*. (2014) 56:182–8. doi: 10.1016/j.exger.2014.01.021
12. White E, Mehnert JM, Chan CS. Autophagy, metabolism, and cancer. *Clin Cancer Res*. (2015) 21:5037–46. doi: 10.1158/1078-0432.CCR-15-0490
13. Gkikas I, Palikaras K, Tavernarakis N. The role of mitophagy in innate immunity. *Front Immunol*. (2018) 9:1283. doi: 10.3389/fimmu.2018.01283
14. Nguyen TD, Shaid S, Vakhrusheva O, KosChade SE, Klann K, Tholken M, et al. Loss of the selective autophagy receptor p62 impairs murine myeloid leukemia progression and mitophagy. *Blood*. (2019) 133:168–79. doi: 10.1182/blood-2018-02-833475
15. Pei S, Minhajuddin M, Adane B, Khan N, Stevens BM, Mack SC, et al. AMPK/FIS1-mediated mitophagy is required for self-renewal of human AML stem cells. *Cell Stem Cell*. (2018) 23:86–100 e6. doi: 10.1016/j.stem.2018.05.021
16. Pollyea DA, Stevens BM, Jones CL, Winters A, Pei S, Minhajuddin M, et al. Venetoclax with azacitidine disrupts energy metabolism and targets leukemia stem cells in patients with acute myeloid leukemia. *Nat Med*. (2018) 24:1859–66. doi: 10.1038/s41591-018-0233-1
17. Dykstra KM, Fay HRS, Massey AC, Yang N, Johnson M, Portwood S, et al. Inhibiting autophagy targets human leukemic stem cells and hypoxic AML blasts by disrupting mitochondrial homeostasis. *Blood Adv*. (2021) 5:2087–100. doi: 10.1182/bloodadvances.2020002666
18. Meyer LM, KosChade SE, Vischedyk JB, Thoenken M, Gubas A, Wegner M, et al. Deciphering the mitophagy receptor network identifies a crucial role for OPTN (optineurin) in acute myeloid leukemia. *Autophagy*. (2023) 19:2982–96. doi: 10.1080/15548627.2023.2230839
19. Qing J, Li C, Hu X, Song W, Tirichen H, Yaigoub H, et al. Differentiation of T helper 17 cells may mediate the abnormal humoral immunity in IgA nephropathy and inflammatory bowel disease based on shared genetic effects. *Front Immunol*. (2022) 13:916934. doi: 10.3389/fimmu.2022.916934
20. Wilkerson MD, Hayes DN. ConsensusClusterPlus: a class discovery tool with confidence assessments and item tracking. *Bioinformatics*. (2010) 26:1572–3. doi: 10.1093/bioinformatics/btq170
21. Ritchie ME, Phipson B, Wu D, Hu Y, Law CW, Shi W, et al. limma powers differential expression analyses for RNA-sequencing and microarray studies. *Nucleic Acids Res*. (2015) 43:e47. doi: 10.1093/nar/gkv007
22. Love MI, Huber W, Anders S. Moderated estimation of fold change and dispersion for RNA-seq data with DESeq2. *Genome Biol*. (2014) 15:550. doi: 10.1186/s13059-014-0550-8
23. Gustavsson EK, Zhang D, Reynolds RH, Garcia-Ruiz S, Ryten M. ggtranscript: an R package for the visualization and interpretation of transcript isoforms using ggplot2. *Bioinformatics*. (2022) 38:3844–6. doi: 10.1093/bioinformatics/btac409
24. Yu G, Wang LG, Han Y, He QY. clusterProfiler: an R package for comparing biological themes among gene clusters. *Omic*. (2012) 16:284–7. doi: 10.1089/omi.2011.0118
25. Wang W, Yu Y, Sun H, Wang Z, Zheng Y, Liang G, et al. Predictive model of postoperative pneumonia after neoadjuvant immunotherapy for esophageal cancer. *J Gastrointest Oncol*. (2022) 13:488–98. doi: 10.21037/jgo-22-149
26. Liu TT, Li R, Huo C, Li JP, Yao J, Ji XL, et al. Identification of CDK2-related immune forecast model and ceRNA in lung adenocarcinoma, a pan-cancer analysis. *Front Cell Dev Biol*. (2021) 9:682002. doi: 10.3389/fcell.2021.682002
27. Obuchowski NA, Bullen JA. Receiver operating characteristic (ROC) curves: review of methods with applications in diagnostic medicine. *Phys Med Biol*. (2018) 63:07TR1. doi: 10.1088/1361-6560/aab4b1
28. Bastrikov NI. Comparative characteristics of different variants in the surgical treatment of blepharoptosis. *Vestn Oftalmol*. (1986) 102:47–8.
29. Cheng R, Xu X. Validation of hepatocellular carcinoma risk prediction models in patients with hepatitis B-related cirrhosis. *J Hepatocell Carcinoma*. (2022) 9:987–97. doi: 10.2147/JHC.S377435
30. McHugh ML. The chi-square test of independence. *Biochem Med (Zagreb)*. (2013) 23:143–9. doi: 10.11613/BM.2013.018
31. Chen B, Khodadoust MS, Liu CL, Newman AM, Alizadeh AA. Profiling tumor infiltrating immune cells with CIBERSORT. *Methods Mol Biol*. (2018) 1711:243–59. doi: 10.1007/978-1-4939-7493-1_12
32. Geleher P, Cox N, Huang RS. pRRophetic: an R package for prediction of clinical chemotherapeutic response from tumor gene expression levels. *PLoS One*. (2014) 9:e107468. doi: 10.1371/journal.pone.0107468
33. Zhang X, Chao P, Zhang L, Xu L, Cui X, Wang S, et al. Single-cell RNA and transcriptome sequencing profiles identify immune-associated key genes in the development of diabetic kidney disease. *Front Immunol*. (2023) 14:1030198. doi: 10.3389/fimmu.2023.1030198
34. KosChade SE, Brandts CH. Selective autophagy in normal and Malignant hematopoiesis. *J Mol Biol*. (2020) 432:261–82. doi: 10.1016/j.jmb.2019.06.025
35. Wai T, Langer T. Mitochondrial dynamics and metabolic regulation. *Trends Endocrinol Metab*. (2016) 27:105–17. doi: 10.1016/j.tem.2015.12.001
36. Rodrigues T, Ferraz LS. Therapeutic potential of targeting mitochondrial dynamics in cancer. *Biochem Pharmacol*. (2020) 182:114282. doi: 10.1016/j.bcp.2020.114282
37. Gao X. Integrated analysis of single-cell RNA-seq and bulk RNA-seq unravels the molecular feature of tumor-associated macrophage of acute myeloid leukemia. *Genet Res (Camb)*. (2024) 2024:5539065. doi: 10.1155/2024/5539065
38. Jian J, Yuan C, Ji C, Hao H, Lu F. DNA methylation-based subtypes of acute myeloid leukemia with distinct prognosis and clinical features. *Clin Exp Med*. (2023) 23:2639–49. doi: 10.1007/s10238-022-00980-4
39. Djajawi TM, Wichmann J, Vervoot SJ, Kearney CJ. Tumor immune evasion: insights from CRISPR screens and future directions. *FEBS J*. (2024) 291:1386–99. doi: 10.1111/febs.17003
40. Severens JF, Karakaslar EO, van der Reijden BA, Sánchez-López E, van den Berg RR, Halkes CJM, et al. Mapping AML heterogeneity - multi-cohort transcriptomic analysis identifies novel clusters and divergent ex-vivo drug responses. *Leukemia*. (2024) 38:751–61. doi: 10.1038/s41375-024-02137-6
41. Zhou Y, Jorgensen JL, Wang SA, Ravandi F, Cortes J, Kantarjian HM, et al. Usefulness of CD11a and CD18 in flow cytometric immunophenotypic analysis for diagnosis of acute promyelocytic leukemia. *Am J Clin Pathol*. (2012) 138:744–50. doi: 10.1309/AJCPQU9R3FSLKFM
42. Laskowska J, Lewandowska-Bieniek J, Szczepanek J, Styczynski J, Tretyn A. Genomic and transcriptomic profiles and *in vitro* resistance to mitoxantrone and idarubicin in pediatric acute leukemias. *J Gene Med*. (2016) 18:165–79. doi: 10.1002/jgm.2889
43. Bi L, Jia S, Hu W, Su X, Chen X, Tang H. Systematic analysis of prognostic significance, functional enrichment and immune implication of STK10 in acute myeloid leukemia. *BMC Med Genomics*. (2022) 15:101. doi: 10.1186/s12920-022-01251-7
44. Iwasaki M, Akiba Y, Kaunitz JD. Recent advances in vasoactive intestinal peptide physiology and pathophysiology: focus on the gastrointestinal system. *F1000Res*. (2019) 8:F1000 Faculty Rev-1629. doi: 10.12688/f1000research
45. Duan JX, Guan XX, Yang HH, Mei WX, Chen P, Tao JH, et al. Vasoactive intestinal peptide attenuates bleomycin-induced murine pulmonary fibrosis by inhibiting epithelial-mesenchymal transition: Restoring autophagy in alveolar epithelial cells. *Int Immunopharmacol*. (2021) 101:108211. doi: 10.1016/j.intimp.2021.108211
46. Zhong HL, Li PZ, Li D, Guan CX, Zhou Y. The role of vasoactive intestinal peptide in pulmonary diseases. *Life Sci*. (2023) 332:122121. doi: 10.1016/j.lfs.2023.122121
47. Yang H, Yang L. Targeting cAMP/PKA pathway for glycemic control and type 2 diabetes therapy. *J Mol Endocrinol*. (2016) 57:R93–r108. doi: 10.1530/JME-15-0316
48. Deng Z, Li X, Blanca Ramirez M, Purcell K, Choi I, Lu JH, et al. Selective autophagy of AKAP11 activates cAMP/PKA to fuel mitochondrial metabolism and tumor cell growth. *Proc Natl Acad Sci U.S.A.* (2021) 118(14):e2020215118. doi: 10.1073/pnas.2020215118
49. Batista S, Maniati E, Reynolds LE, Tavora B, Lees DM, Fernandez I, et al. Haematopoietic focal adhesion kinase deficiency alters haematopoietic homeostasis to drive tumour metastasis. *Nat Commun*. (2014) 5:5054. doi: 10.1038/ncomms6054
50. Weissner M, Yeh RF, Duchateau-Nguyen G, Palermo G, Nguyen TQ, Shi X, et al. PTK2 expression and immunotherapy outcome in chronic lymphocytic leukemia. *Blood*. (2014) 124:420–5. doi: 10.1182/blood-2013-12-538975
51. Fan Z, Duan J, Wang L, Xiao S, Li L, Yan X, et al. PTK2 promotes cancer stem cell traits in hepatocellular carcinoma by activating Wnt/beta-catenin signaling. *Cancer Lett*. (2019) 450:132–43. doi: 10.1016/j.canlet.2019.02.040
52. Khacho M, Slack RS. Mitochondrial and reactive oxygen species signaling coordinate stem cell fate decisions and life long maintenance. *Antioxid Redox Signal*. (2018) 28:1090–101. doi: 10.1089/ars.2017.7228
53. Du W, Xu A, Huang Y, Cao J, Zhu H, Yang B, et al. The role of autophagy in targeted therapy for acute myeloid leukemia. *Autophagy*. (2021) 17:2665–79. doi: 10.1080/15548627.2020.1822628
54. Wang Y, Nartiss Y, Steipe B, McQuibban GA, Kim PK. ROS-induced mitochondrial depolarization initiates PARK2/PARKIN-dependent mitochondrial degradation by autophagy. *Autophagy*. (2012) 8:1462–76. doi: 10.4161/auto.21211

55. Pallares V, Hoyos M, Chillon MC, Barragan E, Prieto Conde MI, Llop M, et al. Focal adhesion genes refine the intermediate-risk cytogenetic classification of acute myeloid leukemia. *Cancers (Basel)*. (2018) 10(11):436. doi: 10.3390/cancers10110436
56. Yan Q, Zhang W, Wu Y, Wu M, Zhang M, Shi X, et al. KLF8 promotes tumorigenesis, invasion and metastasis of colorectal cancer cells by transcriptional activation of FHL2. *Oncotarget*. (2015) 6:25402–17. doi: 10.18632/oncotarget.4517
57. Li SY, Huang PH, Tarng DC, Lin TP, Yang WC, Chang YH, et al. Four-and-a-half LIM domains protein 2 is a coactivator of wnt signaling in diabetic kidney disease. *J Am Soc Nephrol*. (2015) 26:3072–84. doi: 10.1681/ASN.2014100989
58. Wang J, Yang Y, Xia HH, Gu Q, Lin MC, Jiang B, et al. Suppression of FHL2 expression induces cell differentiation and inhibits gastric and colon carcinogenesis. *Gastroenterology*. (2007) 132:1066–76. doi: 10.1053/j.gastro.2006.12.004
59. Pasalic Z, Greif PA, Jurinovic V, Mulaw M, Kakadia PM, Tizazu B, et al. FHL2 interacts with CALM and is highly expressed in acute erythroid leukemia. *Blood Cancer J*. (2011) 1:e42. doi: 10.1038/bcj.2011.40
60. Basu H, Pekkuraj G, Falk J, Wei W, Chin M, Steen J, et al. FHL2 anchors mitochondria to actin and adapts mitochondrial dynamics to glucose supply. *J Cell Biol*. (2021) 220(10):e201912077. doi: 10.1083/jcb.201912077
61. Suzuki M, Iwasaki M, Sugio A, Hishiya A, Tanaka R, Endo T, et al. BAG3 (BCL2-associated athanogene 3) interacts with MMP-2 to positively regulate invasion by ovarian carcinoma cells. *Cancer Lett*. (2011) 303:65–71. doi: 10.1016/j.canlet.2011.01.019
62. Festa M, Del Valle L, Khalili K, Franco R, Scognamiglio G, Graziano V, et al. BAG3 protein is overexpressed in human glioblastoma and is a potential target for therapy. *Am J Pathol*. (2011) 178:2504–12. doi: 10.1016/j.ajpath.2011.02.002
63. Rosati A, Bersani S, Tavano F, Dalla Pozza E, De Marco M, Palmieri M, et al. Expression of the antiapoptotic protein BAG3 is a feature of pancreatic adenocarcinoma and its overexpression is associated with poorer survival. *Am J Pathol*. (2012) 181:1524–9. doi: 10.1016/j.ajpath.2012.07.016
64. Roperto S, Russo V, Rosati A, Ceccarelli DM, Munday JS, Turco MC, et al. Chaperone-assisted selective autophagy in healthy and papillomavirus-associated neoplastic urothelium of cattle. *Vet Microbiol*. (2018) 221:134–42. doi: 10.1016/j.vetmic.2018.06.013
65. Nivon M, Fort L, Muller P, Richet E, Simon S, Guey B, et al. NfκB is a central regulator of protein quality control in response to protein aggregation stresses via autophagy modulation. *Mol Biol Cell*. (2016) 27:1712–27. doi: 10.1091/mbc.e15-12-0835
66. Tang M, Ji C, Pallo S, Rahman I, Johnson GVW. Nrf2 mediates the expression of BAG3 and autophagy cargo adaptor proteins and tau clearance in an age-dependent manner. *Neurobiol Aging*. (2018) 63:128–39. doi: 10.1016/j.neurobiolaging.2017.12.001
67. Das CK, Linder B, Bonn F, Rothweiler F, Dikic I, Michaelis M, et al. BAG3 overexpression and cytoprotective autophagy mediate apoptosis resistance in chemoresistant breast cancer cells. *Neoplasia*. (2018) 20:263–79. doi: 10.1016/j.neo.2018.01.001
68. Hutt DM, Mishra SK, Roth DM, Larsen MB, Angles F, Frizzell RA, et al. Silencing of the Hsp70-specific nucleotide-exchange factor BAG3 corrects the F508del-CFTR variant by restoring autophagy. *J Biol Chem*. (2018) 293:13682–95. doi: 10.1074/jbc.RA118.002607
69. Kögel D, Linder B, Brunschweiler A, Chines S, Behl C. At the crossroads of apoptosis and autophagy: multiple roles of the co-chaperone BAG3 in stress and therapy resistance of cancer. *Cells*. (2020) 9(3):574. doi: 10.3390/cells9030574
70. Körschgen H, Baeken M, Schmitt D, Nagel H, Behl C. Co-chaperone BAG3 enters autophagic pathway via its interaction with microtubule associated protein 1 light chain 3 beta. *Traffic*. (2023) 24:564–75. doi: 10.1111/tra.12916
71. Colvin TA, Gabai VL, Gong J, Calderwood SK, Li H, Gummuluru S, et al. Hsp70-Bag3 interactions regulate cancer-related signaling networks. *Cancer Res*. (2014) 74:4731–40. doi: 10.1158/0008-5472.CAN-14-0747
72. Wang Y, Hu F, Li JY, Nie RC, Chen SL, Cai YY, et al. Systematic construction and validation of a metabolic risk model for prognostic prediction in acute myelogenous leukemia. *Front Oncol*. (2020) 10:540. doi: 10.3389/fonc.2020.00540
73. Randolph TR. Acute promyelocytic leukemia (AML-M3)–Part 2: Molecular defect, DNA diagnosis, and proposed models of leukemogenesis and differentiation therapy. *Clin Lab Sci*. (2000) 13:106–16.
74. Yang Y, Zhao H, Ling G, Liu S, Sun Y, Peng H, et al. Construction and verification of a nomogram model for the risk of death in sepsis patients. *Sci Rep*. (2025) 15:5078. doi: 10.1038/s41598-025-89442-x
75. Ma Y, Zheng S, Xu M, Chen C, He H. Establishing and validating an aging-related prognostic signature in osteosarcoma. *Stem Cells Int*. (2023) 2023:6245160. doi: 10.1155/2023/6245160
76. Zhang J, Wang H, Tian Y, Li T, Zhang W, Ma L, et al. Discovery of a novel lipid metabolism-related gene signature to predict outcomes and the tumor immune microenvironment in gastric cancer by integrated analysis of single-cell and bulk RNA sequencing. *Lipids Health Dis*. (2023) 22:212. doi: 10.1186/s12944-023-01977-y
77. Lasry A, Nadorp B, Fornerod M, Nicolet D, Wu H, Walker CJ, et al. An inflammatory state remodels the immune microenvironment and improves risk stratification in acute myeloid leukemia. *Nat Cancer*. (2023) 4:27–42. doi: 10.1038/s43018-023-00518-x
78. Yu S, Jiang J. Immune infiltration-related genes regulate the progression of AML by invading the bone marrow microenvironment. *Front Immunol*. (2024) 15:1409945. doi: 10.3389/fimmu.2024.1409945
79. Carlino MS, Larkin J, Long GV. Immune checkpoint inhibitors in melanoma. *Lancet*. (2021) 398:1002–14. doi: 10.1016/S0140-6736(21)01206-X
80. Paz-Ares L, Ciuleanu TE, Cobo M, Schenker M, Zurawski B, Menezes J, et al. First-line nivolumab plus ipilimumab combined with two cycles of chemotherapy in patients with non-small-cell lung cancer (CheckMate 9LA): an international, randomised, open-label, phase 3 trial. *Lancet Oncol*. (2021) 22:198–211. doi: 10.1016/S1470-2045(20)30641-0
81. Hellmann MD, Rizvi NA, Goldman JW, Gettinger SN, Borghaei H, Brahmer JR, et al. Nivolumab plus ipilimumab as first-line treatment for advanced non-small-cell lung cancer (CheckMate 012): results of an open-label, phase 1, multicohort study. *Lancet Oncol*. (2017) 18:31–41. doi: 10.1016/S1470-2045(16)30624-6
82. Venkatachalam S, McFarland TR, Agarwal N, Swami U. Immune checkpoint inhibitors in prostate cancer. *Cancers (Basel)*. (2021) 13(9):2187. doi: 10.3390/cancers13092187
83. Ding T, Shang Z, Zhao H, Song R, Xiong J, He C, et al. Anoikis-related gene signatures in colorectal cancer: implications for cell differentiation, immune infiltration, and prognostic prediction. *Sci Rep*. (2024) 14:11525. doi: 10.1038/s41598-024-62370-y
84. Chen R, Wang X, Dai Z, Wang Z, Wu W, Hu Z, et al. TNFSF13 is a novel onco-inflammatory marker and correlates with immune infiltration in gliomas. *Front Immunol*. (2021) 12:713757. doi: 10.3389/fimmu.2021.713757
85. Xia J, Xie Z, Niu G, Lu Z, Wang Z, Xing Y, et al. Single-cell landscape and clinical outcomes of infiltrating B cells in colorectal cancer. *Immunology*. (2023) 168:135–51. doi: 10.1111/imm.13568